2013 IEEE/RSJ International Conference on
Intelligent Robots and Systems (IROS)
November 3-7, 2013. Tokyo, Japan

Modeling and Analysis of Ciliary Micro-Hopping Locomotion Actuated by an Eccentric Motor in a Microgravity*

Kenji Nagaoka[1] and Kazuya Yoshida[1]

Abstract— **This paper presents the modeling and analysis of ciliary micro-hopping locomotion actuated by an eccentric motor, for enabling mobile robots to explore asteroids. Under the proposed system, elastic cilia are attached to the surface of the robot; this arrangement should enable the robot to have better mobility in a microgravity environment. However, in the development of the ciliary micro-hopping mechanism theoretical modeling and analysis of the interactive mechanics between the cilia and the environment pose technical challenges that need to be addressed. In this paper, we present the dynamics modeling of the ciliary micro-hopping locomotion actuated by an eccentric motor, along with its experimental validations and numerical simulations. The results of this study contribute to the design optimization of both the cilia mechanism and the motor control scheme.**

I. Introduction

Locomotion techniques in a microgravity environment constitute a basis of exploration by mobile robots on small celestial bodies. The world's first successful asteroid sample return mission, named Hayabusa, was carried out by the Japan Aerospace Exploration Agency (JAXA). The spacecraft carried a small mobile robot MINERVA (Micro/Nano Experimental Robot Vehicle for Asteroid) [1]. MINERVA possessed hopping mobility and used internal torquers to move around on an asteroid. Unfortunately, MINERVA did not land on the surface because the robot was not released appropriately from the spacecraft. Following the success of the Hayabusa mission, JAXA is now developing a Hayabusa 2 spacecraft. This upcoming mission will explore a more primitive C-type asteroid 162173 (1999 JU3). On the basis of latest observations, the target asteroid has been determined to have an effective diameter of 870±30 m and a rotation period of 7.6 h [2]. The asteroid has also been seen to have an almost spherical shape, and its gravitational acceleration has been nominally estimated to be 1.7×10^{-5} G. In such an uncertain environment, hopping is a promising solution for achieving reliable locomotion on asteroid surfaces in a microgravity environment.

Currently, MINERVA-II [3] and MASCOT (Mobile Asteroid Surface Scout) [4] are being developed as surface probes as part of the Hayabusa 2 mission. In addition to the torquer-type hopping mechanism of MINERVA, several hopping mechanisms have practically been studied in developing these mobile robots. In particular, the MINERVA-II project has encouraged robotics researchers to take up the challenge of developing locomotion systems that can operate under microgravity. Fig. 1 shows a conceptual diagram of an asteroid mission conducted with such a mobile robot. The robot is required to carry out autonomous locomotion and scientific investigation.

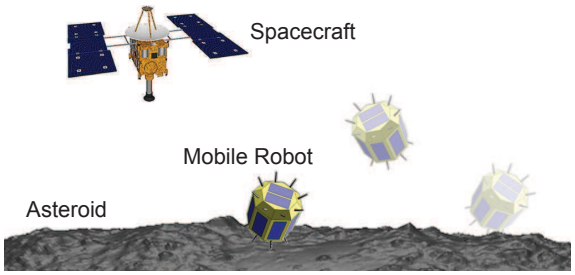

Fig. 1 Artistic Illustration of Asteroid Exploration Mission

Friction-based locomotion gears such as typical wheels or tracks are principally dependent much on a gravitational force. Therefore, such gears are unable to exert sufficient locomotion owing to microgravity. Moreover, they are prone to unexpected hops in rough terrain [5]. Against this background, various hopping mechanisms have been proposed to achieve robotic locomotion on small celestial bodies. The main focus of the past research has been the utilization of an impulsive force such as an internal electro magnetic force [6]; an internal spring force [7], [8]; an external pushing force by whiskers [9], [10] or posable struts [11]; a magnetic force [12]; or a deflection force of a shape memory alloy or bimetal with temperature-dependent change [13]. Even though hopping may be effective on asteroids, large hops will prove to be a drawback to reaching a destination because of the difficulty in building soft-landing gears adaptable to unknown asteroid surfaces.

We proposed an advanced locomotion system that will operate under microgravity; this system is based on ciliary micro-hopping using a high-frequency eccentric motor [14]. Under the proposed system, elastic cilia are attached to the surface of the robot; this arrangement should enable the robot to have better mobility in a microgravity environment. However, in the development of the ciliary micro-hopping mechanism, theoretical modeling and analysis of the interactive mechanics between the cilia and the environment pose technical challenges that need to be addressed. This paper introduces the dynamics models that incorporate linear spring damper models, and then discusses experimental validations of the modeling.

* This work was supported by JSPS KAKENHI Grant Number 60612520.
[1] K. Nagaoka and K. Yoshida are with Department of Aerospace Engineering, Graduate School of Engineering, Tohoku University, Sendai 980–8579, Japan nagaoka@astro.mech.tohoku.ac.jp, yoshida@astro.mech.tohoku.ac.jp

II. Micro-Hopping Locomotion

A. Locomotion Principles

In this section, the principles of micro-hopping locomotion are first summarized. Fig. 2 shows the principles of locomotion under microgravity for typical hopping and micro-hopping. Typical hopping is based on an impulsive force or a rotational force generated inside a mobile robot. Micro-hopping is assumed to be actuated by an eccentric motor whose primary function is to exert a vibrating centrifugal force inside a mobile robot. Furthermore, in the case of micro-hopping, it is assumed that the robot' surface has elastic protrusions (cilia). Such elastic protrusions can also assist in achieving a workable contact duration with the surface and in soft-landing on surfaces. Unlike typical hopping, micro-hopping is continuously repeated at high frequency. Therefore, although one micro-hop represents a small degree of locomotion, the proposed micro-hopping will achieve efficient locomotion over time. Furthermore, the elastic cilia are expected to enhance the controllability of micro-hopping even on uncertain surfaces because contact mechanics can be modeled using the lowest stiffness in the contact system.

On the other hand, there has been some research on the applications of robotic cilia mechanisms [15]–[19] such as for applications for conveyors and actuators. However, from the viewpoint of contact mechanics, this research work does not quite apply to a hopping robot traversing an asteroid. Recently, ciliary vibrating locomotion driven by the centrifugal force of a rotary motor was modeled [15]. The developed models in [15] represented the cilia as a linear spring damper model of bending and deflection. Its fundamental modeling idea can be applied to microgravity environments in many ways. In another application, an active scope camera for help in rescue operations at disaster sites has been developed based on ciliary vibrations [16]. Although this system is a better solution for use in rescue operations, its theoretical modeling is based on the model in [15].

B. Feasibility Test

Prior to the modeling and analysis of the ciliary micro-hopping locomotion, we conducted preliminary experiments to verify the feasibility of the proposed idea. An air-floating test bed equipped with a micro-hopping mechanism was developed to emulate a planar microgravity environment on the ground. The experimental environment and the test bed are shown in Figs. 3(a) and 3(b), respectively. The test bed consisted of electric circuits with power systems, a plastic bottom plate, an air tank, a brushed DC motor with an eccentric mass, and elastic cilia that are made of nylon. The driving component (the motor and the eccentric mass) was attached to the top of the cilia base so that the motor's rotational axis was set in a direction perpendicular to the longitudinal direction of the cilia base. The test bed weighted 1.4 kg. The DC motor was tele-operated with an external laptop via Xbee wireless communication modules. The motor rotational speed was controlled with a pulse-width modulation (PWM) controller implemented on an on-board

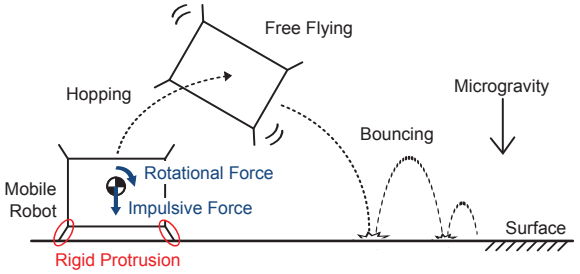

(a) Typical Hopping Locomotion

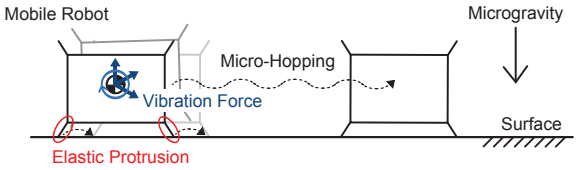

(b) Micro-Hopping Locomotion

Fig. 2 Schematic of Hopping Locomotion Principles

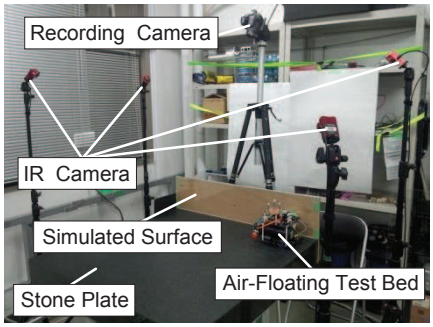

(a) Overview of Experimental Environment

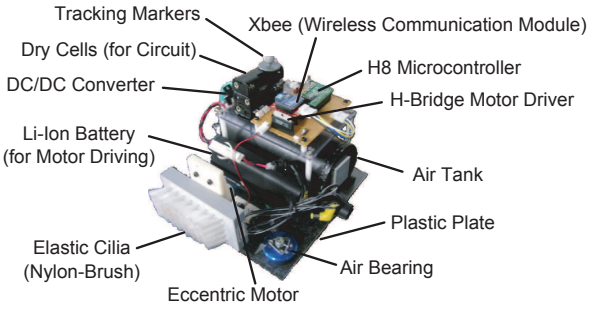

(b) Microgravity-Emulating Test Bed

Fig. 3 Overview of Microgravity Emulating Experiment

H8 microcontroller. The PWM controller is a feed-forward system without any feedback data. The stone plate was set to be slightly tilted to emulate a planar microgravity field. At the end of the plate, an acrylic board was attached as a simulated surface to allow the test bed to move over it.

Fig. 4(a) shows the experimental snapshots, and Fig. 4(b) shows a plot of a time history of the resulting micro-hopping

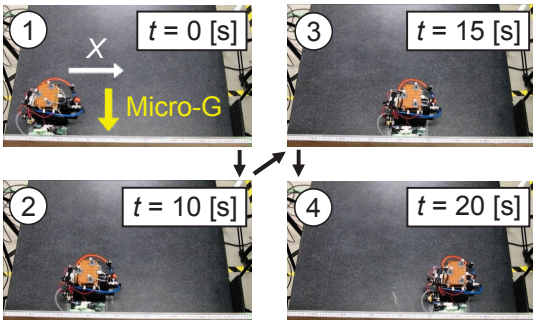

(a) Experimental Snapshots: Locomotion in X-Axis Direction

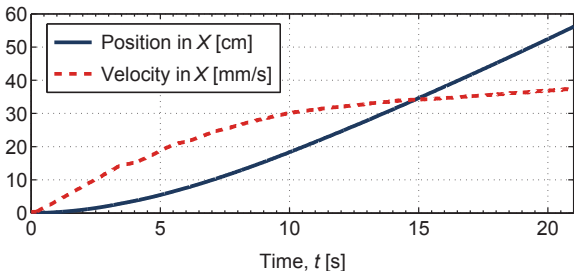

(b) Time History of Position and Velocity in X-Axis Direction

Fig. 4 Ciliary Micro-Hopping Resulted from Microgravity Emulating Experiment

locomotion in the experiment, where we input 100% of the PWM duty cycle. The output velocity in Fig. 4(b) was calculated by processing the position data with a three-dimensional Butterworth low-pass filter. In the experiments, stable micro-hopping locomotion was seen in the X-axis direction. Thus, the feasibility of the proposed micro-hopping was confirmed through ground experiments. The quantitative evaluation of the experiments was detailed in [14]. In particular, the result experimentally confirmed micro-hopping is a possible solution for robotic locomotion under microgravity.

III. Dynamics Modeling

A. Equation of Motion

In this section, we introduce a planar dynamics model of the ciliary micro-hopping robot. The fundamental modeling framework is based on the model in [15]. Fig. 5 shows the schematic of the robot model. The simulated surface is assumed to be unified and flat. At first, $\Sigma_O\{X, Z\}$ is defined as an absolute coordinate system, where X is a horizontal axis parallel to the terrain surface and Z is a vertical axis normal to the terrain. Then, the equations of motion of the robot with n cilia bundles in Σ_O are derived as follows:

$$M\ddot{X}_G = F_{mx} + \sum_{i=1}^{n} \left[F_{ix} - \mathrm{sgn}\left(\dot{p}_{ix}\right)\mu F_{iz}\right] \tag{1}$$

$$M\ddot{Z}_G = F_{mz} - Mg + \sum_{i=1}^{n} F_{iz} \tag{2}$$

$$\begin{aligned} J\ddot{\theta} = \sum_{i=1}^{n} \{ & \left[r_{ix}\cos\theta - r_{iz}\sin\theta - h_i\cos\left(\theta+\phi_i\right)\right] F_{iz} \\ & - \left[r_{ix}\sin\theta + r_{iz}\cos\theta - h_i\sin\left(\theta+\phi_i\right)\right] \\ & \times \left[F_{ix} - \mathrm{sgn}\left(\dot{p}_{ix}\right)\mu F_{iz}\right)\} \\ & + g_{mx}F_{mz} - g_{mz}F_{mx} - \tau_m \end{aligned} \tag{3}$$

where M is the mass of the robot; X_G and Z_G denote the position of the center of mass (COM) of the robot in Σ_O; J is the moment of inertia of the robot around its COM; θ is the rotation angle of the robot around its COM (counter-clockwise is positive); $\mathrm{sgn}\,(\cdot)$ is a signal function; g is the gravitational acceleration; μ is the friction coefficient between the robot and the terrain surface; (g_{mx}, g_{mz}) is the (x, z) position of the point at which the centrifugal force acts on the robot in the robot coordinates $\Sigma_R\{x, z\}$, as shown in Fig. 5(a); (F_{mx}, F_{mz}) is the (x, z) component of the centrifugal force F_m in Σ_R; and (F_{ix}, F_{iz}) is the (x, z) component of the acting force F_i at the root of the i-th cilia. τ_m represents the torque effect of the motor reaction torque τ on the body rotation such that $\tau_m = \tau/r_m$, where r_m is the distance between the COM and a motor shaft axis. With respect to the contact positions, (p_{ix}, p_{iz}) is defined as the tip position of an i-th cilia bundle in Σ_O, where $i = 1, \cdots, n$.

B. Contact Model with Contact Determination

When the cilia do not undergo any elastic deformation, the tip position (p_{ix}, p_{iz}) of the i-th cilia in Σ_O can be geometrically expressed as follows:

$$\begin{cases} p_{ix} = X_G + r_{ix}\cos\theta - r_{iz}\sin\theta - h_i\cos\left(\theta+\phi_i\right) \\ p_{iz} = Z_G + r_{ix}\sin\theta + r_{iz}\cos\theta - h_i\sin\left(\theta+\phi_i\right) \end{cases} \tag{4}$$

where r_{ix} and r_{iz} are the x and z components, respectively, of the cilia-attached position r_i in Σ_R; h_i is the effective cilia length; and ϕ_i is the cilia angle.

Assuming the deformation or buckling of the cilia to be quite small, the reaction force F_i generated by the cilia with upon establishing contact is derived as follows:
(i) $p_{iz} > 0$:

$$F_{ix} = F_{iz} = 0 \tag{5}$$

(ii) $p_{iz} \geq 0$:

$$\begin{cases} F_{ix} = F_{h_i}\cos\left(\theta+\phi_i^*\right) - F_{\phi_i}\sin\left(\theta+\phi_i^*\right) \\ F_{iz} = F_{h_i}\sin\left(\theta+\phi_i^*\right) + F_{\phi_i}\cos\left(\theta+\phi_i^*\right) \end{cases} \tag{6}$$

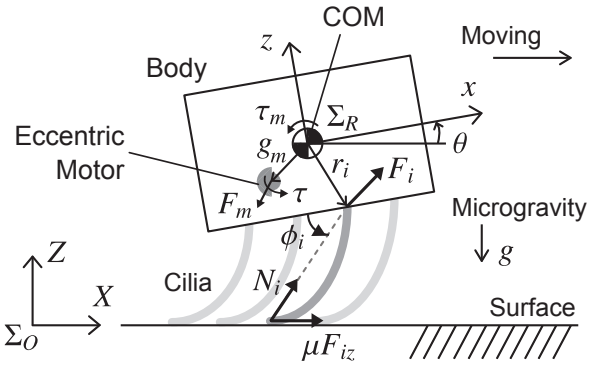

(a) Schematic of Planar Model

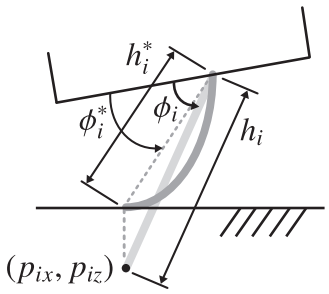

(b) Contact Condition of Cilia

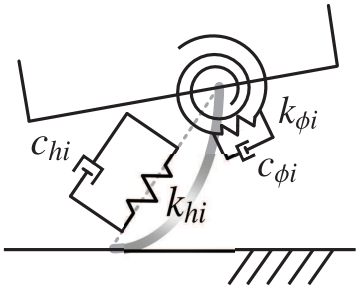

(c) Interactive Mechanics of Cilia and Surface

Fig. 5 Dynamics Model of Ciliary Micro-Hopping Robot

where

Elastic Deflection Force:

$$F_{h_i} = k_{h_i}\left(h_i - h_i^*\right) - c_{h_i}\dot{h_i}^*$$

Rotational Viscoelastic Force:

$$F_{\phi_i} = \frac{k_{\phi_i}\left(\phi_i - \phi_i^*\right) - c_{\phi_i}\dot{\phi_i}^*}{h_i^*}$$

Equivalent Elastic Deformation:

$$h_i^* = h_i + p_{iz}\sin\left(\theta + \phi_i\right)$$

Equivalent Elastic Rotation Angle:

$$\phi_i^* = \phi_i + \frac{p_{iz}\cos\left(\theta + \phi_i\right)}{h_i}$$

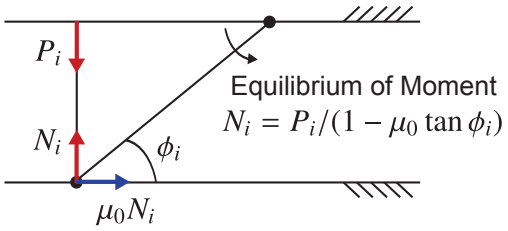

Fig. 6 Schematic Illustration of Frictional Anisotropy

C. Frictional Anisotropy

It is well known that a cantilever-like object diagonally contacts with a simulated surface as if friction has a directionality. These characteristics are attributed to a mechanical factor. Fig. 6 shows the schematic illustration of a frictional anisotropy model. Accordingly, an apparent friction coefficient μ in the direction of sliding is defined as follows:

$$\mu = \begin{cases} \dfrac{\mu_0}{1 + \mu_0 \tan\phi_i} & : \dot{p}_{ix} > 0 \\ \dfrac{\mu_0}{1 - \mu_0 \tan\phi_i} & : \dot{p}_{ix} < 0 \end{cases} \tag{7}$$

where μ_0 is the friction coefficient between the cilia and terrain. It is assumed that both the static and dynamic friction coefficients are identical.

D. Eccentric Motor

The ciliary micro-hopping locomotion is achieved by actuating the eccentric motor. A centrifugal force exerted by an eccentric motor can be represented as follows:

$$\begin{cases} F_{mx} = m r_e \omega^2 \cos\left(\Omega + \theta\right) \\ F_{mz} = m r_e \omega^2 \sin\left(\Omega + \theta\right) \end{cases} \tag{8}$$

where m, r_e, ω, and Ω are the mass of the eccentric mass, the effective length between the rotational axis and COM of the eccentric mass, the motor angular velocity, and the motor angle, respectively. The motor's rotation angle is thus calculated as $\Omega = \int_0^t \omega \cdot dt$, where the initial condition is $\Omega = \Omega_0$ at $t = 0$.

Then, fundamental motor equations are mathematically expressed as a driving source. The proposed system shall have a brushed DC motor for vibrationally rotating an eccentric mass. The equations of the DC motor can generally be given as follows:

$$\tau = K_\tau I_M = J_M \dot{\omega} + \nu_M \omega + \tau_r \tag{9}$$

$$V_M = L_M \dot{I}_M + R_M I_M + K_E \omega \tag{10}$$

where τ is the motor's output torque, J_M is the sum of the inertia of moments of the motor rotor and an eccentric mass, ν_M is the motor's damping coefficient, τ_r is the external torque resistance, K_τ is the torque constant, I_M is the motor current, L_M is the motor's inductance, R_M is the inner resistance, K_E is a back electromotive force constant, and V_M is the input voltage. The motor does not have a gear head

attached; hence, in this case, the motor ideally drives with the condition $\nu_M = 0$. Although the resistance torque exerted by the eccentric mass can be expressed as $\tau_r = mgr_e \cos\Omega$, we assume $\tau_r \approx 0$ because of the microgravity environment.

Moreover, we assume $V_M \approx R_M I_M + K_E\omega$ in the subsequent analysis model because a motor's eccentric time constant L_M/R_M is generally larger than that of the motor rotational velocity ω. As such, $\dot{\omega}$ and τ can be written as follows:

$$\begin{cases} \dot{\omega} = \dfrac{K_\tau}{J_M R_M}\left(V_M - K_E\omega\right) \\ \tau = \dfrac{K_\tau}{R_M}\left(V_M - K_E\omega\right) \end{cases} \tag{11}$$

Given that V_M is constant, solving the first-order differential equation for ω in (11) provides ω and τ in the following time-dependent representations. The motor is, in effect, driven by the PWM controller. Thus, the motor input voltage V_M can be pseudo-constant.

$$\begin{cases} \omega = \dfrac{V_M}{K_E}\left[1 - \exp\left(-\dfrac{K_\tau K_E}{J_M R_M}t\right)\right] \\ \tau = \dfrac{K_\tau V_M}{R_M}\exp\left(-\dfrac{K_\tau K_E}{J_M R_M}t\right) \end{cases} \tag{12}$$

Accordingly, (8) and (11) or (12) provide driving outputs of the ideal eccentric motor.

IV. Experimental Validation

A. Experimental Setup and Preliminary Measurements

An overview of the experimental system was previously shown in Fig. 3(b) and 3(a). Fig. 7 shows the experimentally determined relationship between the cilia vibrating frequency and the PWM duty cycle that was input to the test bed. Here, the vibrations of the cilia induced by the motor were directly measured by a vibration sensor mounted on the cilia base. The sensor data was processed using fast Fourier transform (FFT) to determine the frequency. Fig. 7 shows the resulting relationship between the motor vibrating frequency estimation and the PWM duty cycle input to the test bed. The result confirmed that the relationship was almost linear.

B. Parameters in Simulation Analysis

TABLE I lists the simulation parameters based on the experimental setup, where X_{G0} and Y_{G0} are the initial positions of X_G and Y_G, respectively. The robot and cilia parameters were basically determined so as to match the test bed specifications. Some kinematic or dynamic cilia parameters were determined experimentally based on a relationship between the static load and the deformation of the cilia unit. At an initial time $t = 0$, the simulations assumed $\dot{X}_{G0} = \ddot{X}_{G0}$ [m/s^2] and $\dot{Y}_{G0} = \ddot{Y}_{G0} = 0$ [m/s]. For simplifying the analysis, g_{mx} and g_{mz} were set to zero according to the configuration of the test bed. The cilia parameters were considered identical for all cilia bundles. To simulate the motor behaviors, we used actual specifications

TABLE I Simulation Parameters

Robot Variable	Value	Cilia Variable	Value
M	1.4 kg	n	8
J	0.02 kgm^2	h_i	0.01596 m
g	5.0^{-4} m/s^2	r_m	0.003 m
m	0.0012 kg	r_{ix}	0.035–0.01i m
μ_0	0.23	r_{iz}	0.02 m
X_{G0}	0.05 m	ϕ_i	70°
X_{G0}	0.0345 m	K_{h_i}	2×10^3 N/m
g_{mx}	0 m	c_{h_i}	0.1 Ns/m
g_{mz}	0 m	K_{ϕ_i}	1×10^{-5} Nm/rad
		c_{ϕ_i}	1×10^{-5} Nms/rad

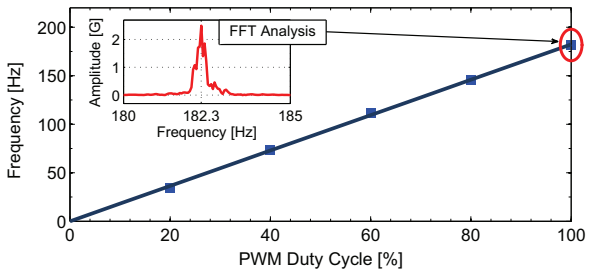

Fig. 7 Approximated Motor Frequency with FFT of Vibration Sensor Data

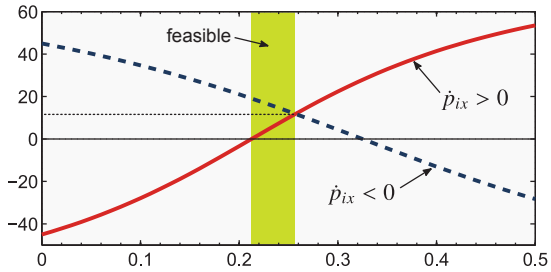

Fig. 8 Identification of Friction Coefficient

of brushed DC motor of the test bed (RE-max13 produced Maxon Motor ag.); $K_E = 3.39\times10^{-3}$ [Nm/A], $\Omega_0 = 0$ [rad], and $R_M = 11$ [Ω]. Here, J_M was also 3.06×10^{-8} kgm^2. As regards to the control law of the motor, the feed-forward PWM controller as well as the test bed was applied.

The characteristics of friction between the cilia and the surface are key factors in the simulation analysis. Through experimental identification, the friction coefficient here was determined such that the simulation results matched the experimental results. Fig. 8 shows the friction coefficient between the nylon cilia, as obtained in the experimental results. The identification experiments were carried out using only the cilia unit. In the experiments, the cilia unit was statically placed on a tilted acrylic slope. Then, to determine the frictional characteristics, we measured the slope angle at the time the cilia unit started to move. Consequently, by substituting the slope angle as the angle of friction in (7),

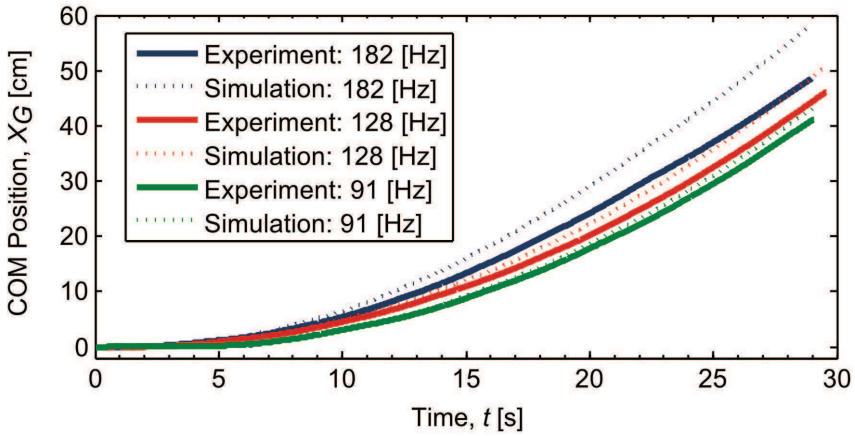

Fig. 9 Comparative Analysis Result of Experimental Data and Simulation Plots

we obtain the friction coefficient.

C. Results and Discussion

Fig. 9 shows the results of the comparative analysis between the experimental data and the simulation plots. The graph depicts only time histories of the COM's locomotion position in the X-axis direction. The simulation results mathematically confirmed that ciliary micro-hopping locomotion can be achieved in a microgravity environment. The simulation results obtained on the basis of the model are qualitatively consistent with the experimental results. However, quantitatively, the two results do not completely match. The difference between the two results can be reduced by using a reasonable parameter tuning approach.

V. Conclusions

This paper described the theoretical modeling and analysis of ciliary micro-hopping locomotion actuated by an eccentric motor. The model was developed using linear spring damper models, and the motor's transitional conditions were also considered. As a result, ciliary micro-hopping locomotion was able to be mathematically represented, and thus be applied to a microgravity experiment. The model was validated by performing a comparative analysis of the experiments using an air-floating test bed. The next stage in the development of the proposed ciliary micro-hopping system entails working on quantitative improvements of the model to obtain feedback regarding design optimization and control. In addition, more challenging rough terrain of an asteroid including rocks or obstacles should be addressed.

References

[1] T. Yoshimitsu, T. Kubota, I. Nakatani, T. Adachi, and H. Saito, "Micro-hopping robot for asteroid exploration," *Acta Astronaut.*, Vol. 52, No. 2–6, pp. 441–446, 2003.

[2] T. G. Müller, et al., "Thermo-physical properties of 162173 (1999 JU3), a potential flyby and rendezvous target for interplanetary missions," *Astron. Astrophys.*, Vol. 525, A145, 2011.

[3] T. Yoshimitsu, T. Kubota, T. Adachi, and Y. Kuroda, "Advanced robotic system of hopping rovers for small solar system bodies," in *Proc. 11th Int. Symp. Artif. Intel., Robot. Autom. in Space*, Turin, Italy, 6A-01, 2012.

[4] C. Dietze, et al., "Landing and mobility concept for the small asteroid lander MASCOT on asteroid 1999 JU3," in *Proc. 61st Int. Astronaut. Cong.*, Prague, Czech Republic, IAC-10.A3.5.8, 2010.

[5] K. Takahashi, S. Shimoda, K. Iizuka, T. Kubota, and I. Nakatani, "A study of locomotion mechanism based on gravitational environment," in *Proc. 2004 IEEE/RSJ Int. Conf. Intel. Rob. Syst.*, Sendal, Japan, 2004, pp. 4001–4006.

[6] Y. Nakamura, S. Shimoda, and S. Shoji, "Mobility of a microgravity rover using internal electro-magnetic levitation," in *Proc. 2010 IEEE/RSJ Int. Conf. Intel. Rob. Syst.*, Taipei, Taiwan, 2000, pp. 1639–1645.

[7] J. Burdick and P. Fiorini, "Minimalist jumping robots for celestial exploration," *Int. J. Robot. Res.*, Vol. 22, No. 78, pp. 653–674, 2003.

[8] S. Shimoda, T. Kubota, and I. Nakratani, "New mobility system based on elastic energy under microgravity," in *Proc. 2002 IEEE Int. Conf. Robot. Autom.*, Washington, DC, 2002, pp. 2296–2301.

[9] K. Yoshida, "The jumping tortoise: A robot design for locomotion on micro gravity surface," in *Proc. 5th Int. Symp. Artif. Intel., Robot. Autom. in Space*, Noordwijk, The Netherlands, 1999, pp. 705–707.

[10] S. Ulamec, V. Kucherenko, J. Biele, A. Bogatchev, A. Makurin, and S. Matrossov, "Hopper concepts for small body landers," *Adv. Space Res.*, Vol. 47, No. 3, pp. 428–439, 2011.

[11] B. H. Wilcox and R. N. Jones, "The MUSES-CN nanorover mission and related technology," in *Proc. 2000 IEEE Aerospace Conf.*, Big Sky, MT, 2000, Vol. 7, pp. 287–295.

[12] M. Kurisu, "Novel hopping mechanism using permanent magnets for tiny asteroid exploration rover," in *Proc. 11th Int. Symp. Artif. Intel., Robot. Autom. in Space*, Turin, Italy, 6A-03, 2012.

[13] Y. Tsumaki, T. Akaike, R. Kazama, T. Mineta, and R. Tadakuma, "Environment-driven rover for asteroid exploration," in *Proc. 11th Int. Symp. Artif. Intel., Robot. Autom. in Space*, Turin, Italy, P-20, 2012.

[14] K. Nagaoka, R. Takano, T. Izumo, and K. Yoshida, "Ciliary micro-hopping locomotion of an asteroid exploration robot," in *Proc. 11th Int. Symp. Artif. Intel., Robot. Autom. in Space*, Turin, Italy, 6A-04, 2012.

[15] K. Ioi, "A mobile micro-robot using centrifugal forces," in *Proc. 1999 IEEE/ASME Int. Conf. Adv. Intel. Mechatr.*, Atlanta, GA, 1999, pp. 736–741.

[16] M. Konyo, K. Isaki, K. Hatazaki, S. Tadokoro, and F. Takemura, "Ciliary vibration drive mechanism for active scope cameras," *J. Robot. Mechatr.*, Vol. 20, No. 3, pp. 490–499, 2008.

[17] W. Mansour, M. Massoud, W. Morcos, and C. Lauzier, "The mechanism of conveyance with bristled tracks," *Trans. ASME, J. Eng. Indust.*, Vol. 97, No. 1, pp. 167–174, 1975.

[18] T. Hatsuzawa, M. Hayase, and T. Oguchi, "A linear actuator based on cilia vibration," *Sens. Actuators A: Phys.*, Vol. 105, No. 2, pp. 183–189, 2003.

[19] Z. Ding and B. Ziaie, "Vibration-induced frequency-controllable bidirectional locomotion for assembly and microrobotic applications," *IEEE Trans. Robot.*, Vol. 25, No. 5, pp. 1192–1196, 2009.